Journal of Science and Technology – Engineering and Technology for Sustainable Development
Volume 36, Issue 5, November 2026, 103–115

A Cost-Optimized Electroencephalogram-Based Brain–Computer Interfaces System for Eye-Blink Behavior Recognition Using Convolutional Block Attention-FusionNet

Viet Ngo Ba[1], Hai Nguyen Thanh[1,*], Nghia Nguyen Thanh[1], Tan Tran Duc[2], Nghiep Chu Thi[3]
[1]HCMC University of Technology and Engineering, Ho Chi Minh City, Vietnam
[2]Phenikaa University, Ha Noi, Vietnam
[3]Brain-Life Link Technology Joint Stock Company, Ho Chi Minh City, Vietnam
[*]Corresponding author email: nthai@hcmute.edu.vn

Abstract

Electroencephalogram (EEG) signals in the field of Brain–Computer Interfaces (BCI) are increasingly being explored for research purposes, intelligent device control, behavior recognition, and supporting users in contactless interactions. To address the demands of BCI applications, this study proposes an eye-blink signal acquisition device based on EEG signals with key characteristics including compact size, low cost, and high accuracy. In parallel, a deep learning model based on a one-dimensional Convolutional Neural Network (1D-CNN) integrated with the proposed CBA-FusionNet architecture combining a Convolutional Neural Network (CNN), a Bidirectional Long Short-Term Memory (BiLSTM) network, and an Attention mechanism is developed to maximize the classification performance of eye-blink signals corresponding to four specific behaviors: left-eye blink (L), right-eye blink (R), simultaneous blinking of both eyes (B), and the neutral state (N). Specifically, the designed two-channel hardware platform demonstrates comfortable wearability and stable continuous operation under practical conditions, reliably capturing blink signals that exhibit characteristic sharp peaks. The acquired bio-signals were formulated into a dedicated dataset across the four eye-movement classes (L, R, B, and N) to validate the end-to-end processing pipeline. Experimental evaluations demonstrate that the system achieves an average classification accuracy of 96% during training and maintains 90.5% in real-world testing environments. By integrating the signal acquisition hardware with CNN-based signal processing software, the proposed system forms a complete framework with potential applications in contactless control interfaces and user-assistive devices.

Keywords: Brain–computer interface (BCI), eye-blink recognition, electroencephalogram (EEG), 1D-CNN.

1. Introduction

Today, neuroscience is a field attracting significant interest due to its complexity and applications related to life as well as smart devices [1]. Therefore, electroencephalogram (EEG) is the primary technological tool used to capture signals for analyzing brain electrical activity in a non-invasive manner, by attaching electrodes to the scalp [2]. This approach allows the system to record signals emitted by the cerebral cortex during human processes such as thinking, emotions, movement, or responses to the environment. Furthermore, EEG is applied in the diagnosis and detection of abnormal brain conditions [3]. EEG not only plays a crucial role in diagnosing neurological disorders but also serves as the foundation for modern Brain–Computer Interface (BCI) research [4]. This represents an advanced approach that enables humans to interact with external devices using only brain signals, particularly benefiting individuals who have lost motor abilities but retain cognitive function.

EEG signals record the bioelectrical activity of the brain and are widely used because of their non-invasive nature, relatively low cost, and ability to capture brain activity in real time. However, EEG signals are highly susceptible to noise from low-frequency power sources and physiological activities of the body. Among these, eye movements and eye blinks generate characteristic electrical signals that often appear as artifacts in EEG recordings, particularly in the frontal region. EEG signals can also be used to evaluate eye activity for disease detection or device control, such as controlling electric wheelchairs [5]. Although traditionally treated as noise and removed during signal processing, recent studies indicate that eye blink signals contain distinctive information that can be utilized for behavior recognition and device control, especially through features such as low-frequency oscillations and sharp artifacts associated with eyelid movements [6, 7].

BCI systems commonly utilize EEG signals to translate brain activity or related physiological responses into control commands for external devices. In BCI applications, EEG can encode cognitive states, control intentions, or evoke responses such as P300 and Steady-State Visually Evoked Potential (SSVEP),

p-ISSN 3093-3242
e-ISSN 3093-3579
https://doi.org/10.51316/jst.195.etsd.2026.36.5.13
Received: Mar 11, 2026; Revised: May 26, 2026;
Accepted: Jul 2, 2026; Online: Oct 30, 2026

enabling users to interact with computers, robots, or smart environments [8]. EEG-based BCI has been widely applied in assistive technologies for people with disabilities, as well as in smart homes, rehabilitation, and entertainment systems [9, 10]. Current research also focuses on developing low-cost and wearable EEG-BCI systems with efficient signal processing methods, making practical non-contact interaction and real-world applications more accessible [11].

The development of deep learning has strongly promoted the application of Convolutional Neural Network (CNN) models and deep architectures in EEG signal analysis for BCI [12]. Specifically, CNN models have the ability to automatically extract spatio-temporal features from raw EEG signals or transformed EEG signals. Specifically, the results of the CNN model have improved classification accuracy for all subjects by 2.37% to 28.28%. It is evident that the classification performance is superior compared to traditional machine learning methods based on manual feature extraction for certain tasks such as motor imagery or cognitive state recognition. In many recent studies, there is a trend of shifting from classical methods to CNN architectures, CNN - Long Short - Term Memory (LSTM), and other deep learning variants to leverage the sequential structure and complex nonlinearity of EEG signals in modern BCI systems [13, 14].

A recent advanced research direction employs a One-Dimensional CNN (1D-CNN) model integrated within a hybrid Convolutional Block Attention (CBA)-FusionNet architecture, combining CNN, Bidirectional LSTM (BiLSTM), and Attention mechanisms to maximize EEG signal classification performance [15]. Specifically, hybrid models are used for recognizing or classifying eye blink signals according to specific behaviors. In similar hybrid models, 1D-CNN handles local temporal feature extraction, BiLSTM captures bidirectional long-term dependencies in EEG sequences, while Attention highlights the most critical signal segments for the classification task. With this model, accuracy and generalization capability are significantly improved [16]. Recent works on eye blink and blink-related EEG classification demonstrate that CNN/BiLSTM/ Attention-based approaches can reliably distinguish states such as no blink, single blink, consecutive blinks, or intentional blinks, thereby suitable for encoding multiple control commands in BCI [17].

When combining EEG acquisition hardware such as wearable EEG devices with minimal electrode setups; CNN-based processing and classification software; and related deep learning architectures, a complete system can be built for non-contact control interfaces and user support devices [18]. Specifically, reviews of wearable BCI devices indicate a trend toward tight integration between signal acquisition hardware, real-time processing pipelines, and deep learning modules on edge devices or the cloud, enabling BCI deployment in everyday life contexts. Thanks to the scalability of both hardware and deep learning models, EEG-CNN systems can be customized for various applications [19]. Thus, with this model type, several assistive systems for the disabled and next-generation human-machine interfaces can be created [20].

Thus, building a classification model for eye blink signals according to specific behaviors-including left eye blink (increased amplitude in the right channel), right eye blink (increased amplitude in the left channel), simultaneous blink of both eyes (bilateral symmetry), and no-blink state (low baseline)-is entirely feasible. The use of combined techniques such as Continuous Wavelet Transform (CWT), 1D-CNN, or hybrid CNN-RNN to achieve high accuracy (above 90%) in multi-class BCI applications is entirely feasible [21, 22]. Specifically, some authors have developed three machine learning models such as XGBoost, Support Vector Machine (SVM), and Neural Network using EEG eye blink signals and achieved a maximum accuracy of 89.0%, while the You Only Look Once (YOLO) model achieved an accuracy of 95.39% [23]. The key issue is that designing hardware combined with intelligent techniques for low-cost EEG signal acquisition and processing is highly meaningful.

Therefore, this study proposes the design and development of an EEG-based blink detection device using a two-channel configuration with five electrodes positioned on the frontal region. This configuration is suitable for mobile systems and is capable of achieving blink detection accuracy of approximately 96%, comparable to more complex multi-channel EEG/ Electrooculography (EOG) systems [24]. The device is designed to acquire and record characteristic blink-related EEG features, including high-amplitude peaks appearing in the frontal region with durations of approximately 200–400 ms. In addition, the system supports real-time storage of blink EEG data via SD card or USB for further analysis and future applications [25].

2. Proposed Method

2.1. Electroencephalogram Signal Acquisition Circuit Design

The hardware for acquiring, amplifying, and filtering the eye-blink signal is presented in Fig. 1, which illustrates the block diagram of the bio-signal acquisition circuit. The signal is collected from electrodes attached to the body, and the entire system is powered by a power module. The circuit consists of two independent measurement channels (Channel 1 and Channel 2). In each channel, the differential signal is first amplified by a differential amplifier to enhance the useful signal and suppress common-mode noise. The signal then passes through filtering and amplification stages to improve its quality before being delivered to the corresponding output.

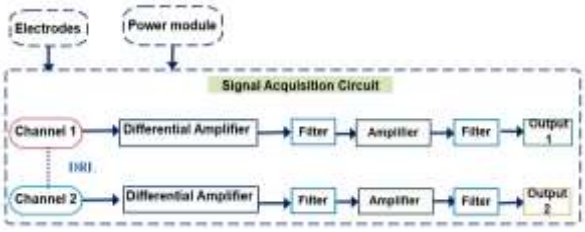


Fig. 1. The EEG acquisition circuit for eye blink activity consisting of 2 channels and 5 electrodes

The diagram also integrates a Driven Right Leg (DRL) circuit to improve measurement quality. This circuit extracts the common-mode noise from the amplifier inputs, inverts it, and feeds it back to the body. This negative feedback mechanism stabilizes the reference potential, reduces 50/60 Hz power-line interference, improves the common-mode rejection ratio (CMRR), and prevents amplifier saturation. As a result, the output bio-signal achieves higher accuracy and reliability, meeting the requirements of systems such as Electrocardiogram (ECG), EEG, or Electromyography (EMG).

2.1.1. Electrodes for electroencephalogram signal acquisition

The electrodes used are from the Emotiv EPOC+ system (see Fig. 2). They are circular disc-shaped electrodes with a concave center (cup electrodes). The gold-colored disc is gold-plated to enhance conductivity and reduce noise, while the silver wire is insulated with a plastic coating and long enough to connect from the scalp to the EEG recording device. These electrodes are suitable for brain activity research, neurological diagnosis, and BCI applications due to their high accuracy and reliability. After measurements, they should be cleaned with antiseptic alcohol to prevent oxidation. The concave center design allows conductive gel to be added when necessary to improve signal quality.



Fig. 2. Electrodes for EEG signal acquisition

2.1.2. Differential amplifier block

The measurement amplifier comprises a buffer amplifier, a differential amplifier, and a power amplifier, thereby significantly boosting the overall gain while effectively suppressing common-mode noise through a high CMRR. Fig. 3 illustrates the INA128 instrumentation amplifier, whose gain can be easily adjusted by changing the value of an external resistor. By modifying the gain, the amplification level of the input EEG signal can be adjusted, making it easier to observe and analyze.

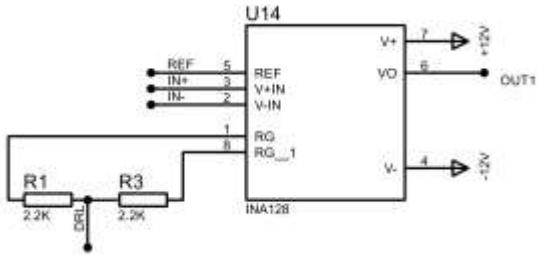


Fig. 3. INA128 schematic diagram

The gain of the INA128 is calculated using the following formula:

$$G = 1 + \frac{50k\Omega}{R_G} \quad (1)$$

By selecting G = 12, the circuit amplifies the input signal 12 times before passing it to the subsequent stages. From (1), it can be derived that R_G is equal approximatly $4{,}55k\Omega$. Here, two 2.2 kΩ resistors connected in series are selected for R_G.

In practice, the output voltage of the amplifier is calculated using the following formula:

$$V_o = (V_{in+} - V_{in-})G + \frac{1}{2}A_{cm}(V_{in+} - V_{in-}) \quad (2)$$

where A_{cm} is the common-mode gain, and the *CMRR* (dB) value is calculated using the following formula:

$$CMRR = 10log_{10}(\frac{G}{|Acm|}) \quad (3)$$

With a gain of 12 and an operating frequency around 100 Hz, the *CMRR* is approximately 105 dB. Substituting this value into (3), the common-mode gain A_{cm} is obtained at about 8.5. Therefore, according to (2), the expected actual output voltage of the INA128 is approximately V_o = 33 mV. To minimize the influence of common-mode noise, achieving a high CMRR is essential.

2.1.3. Sallen – key filter

Two low-pass and high-pass filters are designed using the second-order Sallen–Key topology, as the Sallen–Key filter is well suited for biomedical electronic circuits. Fig. 4 shows the Sallen–Key low-pass filter, with the formulas for calculating the gain K and the cutoff frequency f_c given as follows:

$$K = 1 + \frac{R_4}{R_3} \quad (4)$$

$$f_c = \frac{1}{2\pi\sqrt{R_1R_2C_1C_2}} \quad (5)$$

K is chosen as 1 because the circuit does not provide amplification. Therefore, resistors R_3 and R_4 are omitted. In this study, a band-pass filter with a frequency range of 0.4–106 Hz is required; hence, the cutoff frequency of the Sallen–Key low-pass filter is set to

106 Hz. With $f_c = 106\text{Hz}$, based on (5), the selected component values are $R_1 = R_2 = 15\ k\Omega$ and $C_1 = C_2 = 0.1\ \mu F$.

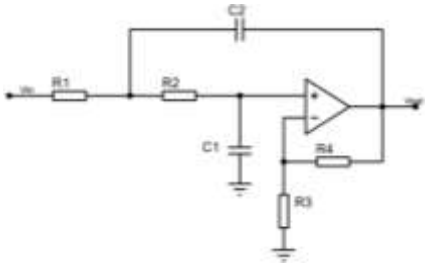


Fig. 4. Sallen–Key low-pass filter circuit

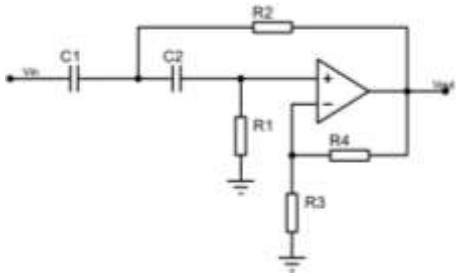


Fig. 5. Sallen–Key high-pass filter circuit

Fig. 5 illustrates the Sallen–Key high-pass filter. In this case, the cutoff frequency of the Sallen–Key high-pass filter is set to 0.4 Hz. Based on (5), the selected values are $R_1 = R_2 = 3.9\ M\Omega$ and $C_1 = C_2 = 0.1\ \mu F$. Resistors R_3 and R_4 are also omitted.

2.1.4. Main amplifier circuit

After passing through the differential amplifier and the filters, the input signal needs to be further amplified, as it may have been attenuated. Fig. 6 illustrates the main amplifier circuit, with the gain calculated as follows:

$$G_A = \frac{R_2}{R_1} + 1 \tag{6}$$

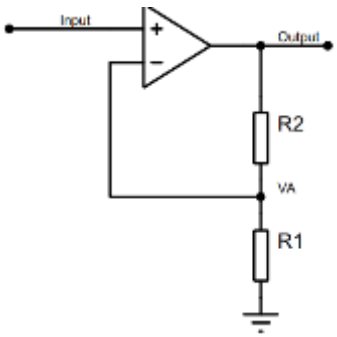


Fig. 6. Main amplifier circuit schematic

The main amplifier provides an approximate gain of 22 times. From (6), with $R_{12} = 100\ k\Omega$, it follows that $R_{11} \approx 4.7\ k\Omega$.

In addition, after passing through the Sallen–Key band-pass filter, the signal is further amplified by approximately 11 times before entering the notch filter. The gain is calculated similarly to that of the main amplifier, and the selected components are shown in Fig. 7.

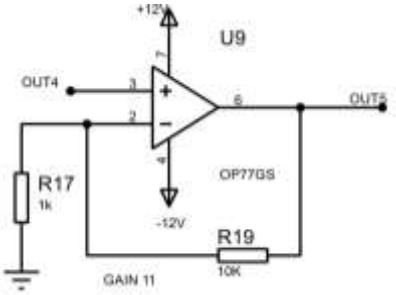


Fig. 7. Final-stage amplifier circuit schematic

2.1.5. Notch filter

The notch filter circuit shown in Fig. 8 is used to eliminate interference at a specific frequency, typically 50 Hz or 60 Hz from the power line. This filter helps reduce power-line noise, thereby improving the clarity and accuracy of the EEG signal. The notch frequency and the gain of the notch filter are calculated using the following formulas:

$$f_{tr} = \frac{1}{4\pi R_0 C_0} \tag{7}$$

$$K = 1 + \frac{R_{Q1}}{R_{Q2}} \tag{8}$$

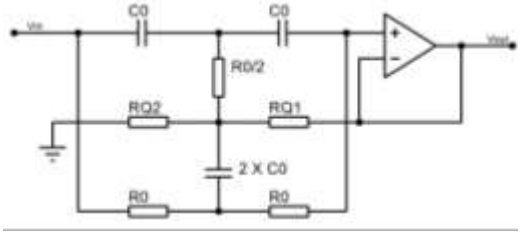


Fig. 8. Notch filter

Since the filter does not provide amplification, R_{Q1} and R_{Q2} are not required. Because the power-line frequency is 50 Hz, the notch (rejection) frequency of the band-stop filter is set to $f_{tr} = 50\text{Hz}$. From (7), the selected values are $R_0 = 68\ k\Omega$ and $C_0 = 47\ nF$.

2.1.6. Driven right leg circuit

The Driven Right Leg (DRL) circuit is very important in biomedical signal recording systems, especially in EEG, because it helps reduce the common-mode voltage between the subject's body and the amplifier circuit [26, 27]. By bringing the body to the same reference potential as the amplifier, the DRL improves noise rejection capability, enhances the quality of the acquired signal, and minimizes the effects of

leakage currents or interference from external sources.

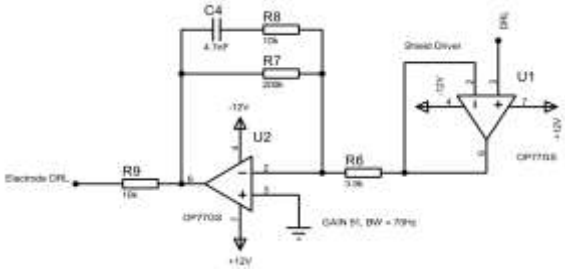


Fig. 9. Schematic of the DRL circuit

Fig. 9 shows the schematic of a DRL circuit commonly used in biomedical signal measurement systems such as EEG or ECG. The purpose of the DRL circuit is to reduce common-mode noise and improve signal quality. When the body is exposed to environmental interference (e.g., 50 Hz or 60 Hz power-line noise), these signals are sensed at both inputs of the biomedical acquisition system. The DRL circuit amplifies the common-mode noise and feeds an inverted signal back to the body through the DRL electrode, thereby reducing the common-mode components in the measured signal. The DRL circuit plays a crucial role in minimizing electrical interference and improving data reliability during biomedical signal recording. As shown in Fig. 9, the DRL circuit is designed with a gain of 21 and operates mainly in the frequency range below 70 Hz, making it suitable for suppressing high-frequency noise without affecting important biological signals.

2.1.7. Schematic diagram

Fig. 10 illustrates an EEG acquisition and processing system consisting of two independent channels (CH1 and CH2). Each channel includes a differential amplifier, band-pass filter, additional gain stage, and a Notch filter to ensure a clean and clear signal. The low-amplitude EEG signal is fed through J3 (CH1) and J4 (CH2), passes through a protection circuit against overvoltage and high-frequency noise, and is then amplified by the INA128 with a gain set by RG.

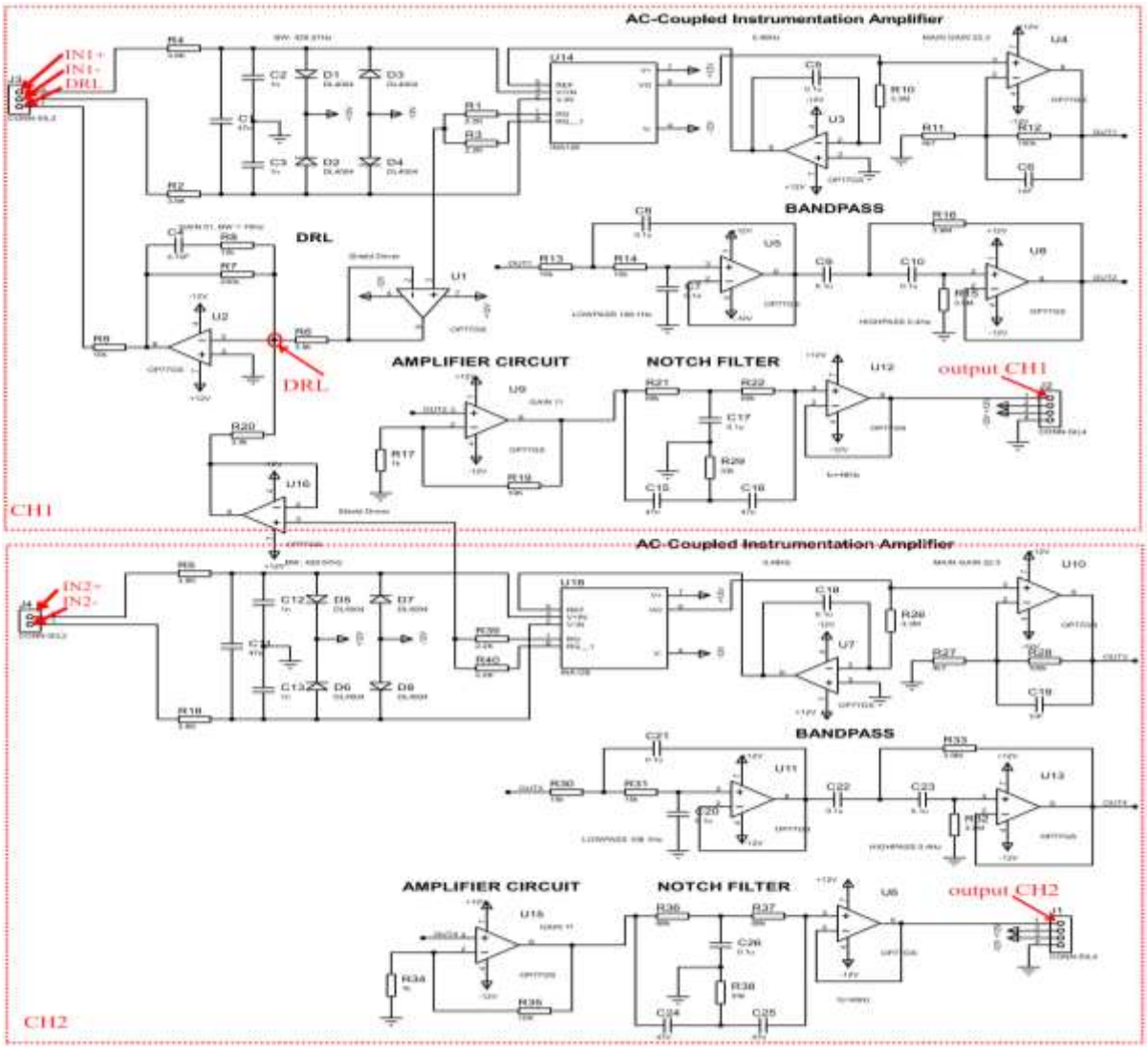


Fig. 10. EEG signal acquisition circuit with two channels

The signal is AC-coupled to remove the DC component and then passed through a band-pass filter (0.4–106 Hz) to retain the EEG frequency range of interest. It is further amplified 11 times and processed by a 50 Hz Notch filter to eliminate power-line interference. Channel CH1 integrates a DRL circuit to suppress common-mode noise and stabilize body potential, while CH2 shares the same DRL electrode. Finally, the processed signals are output through OUT1 and OUT2 for transmission to a computer for analysis.

2.2. Classification Model of Electroencephalogram Signals for Eye-Blink Activity

This study develops a 1D-CNN model to predict four eye movements: left blink (L – Left), right blink (R – Right), both-eye blink (B – Both), and no blink (N – Neutral). Fig. 11 illustrates the blink signal classification model in detail. During the training phase, data are collected from the designed signal acquisition circuit, then labeled, standardized, and preprocessed before being used for model training.

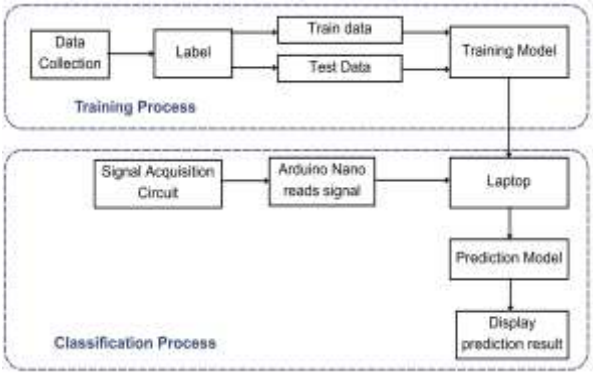


Fig. 11. Signal classification system block diagram

2.2.1. Data collection

The dataset used for training was self-collected using a low-cost two-channel EEG signal acquisition device designed by the research team. The dataset consists of 1000 signal samples corresponding to four eye movements: L, R, B, and N, with each movement containing 250 samples. Data were recorded at a sampling frequency of 128 Hz through multiple acquisition protocols, each lasting 65 seconds, as illustrated in Fig. 12. To evaluate the effectiveness of the proposed EEG device, four participants (2 males and 2 females aged between 20 and 22) were recruited for the experiments. Before the data collection process, all participants were fully informed about the experimental stages and procedures.

The dataset contains 1280 columns, where the first 640 columns correspond to samples from Channel 1, and the next 640 columns correspond to Channel 2. The dataset is divided into two subsets: 80% for training and 20% for testing as in Table 1.

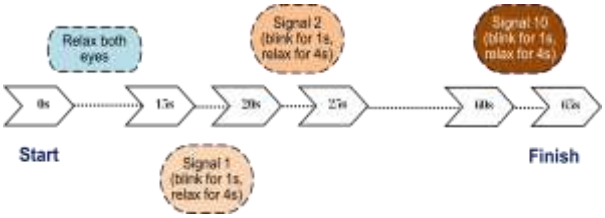


Fig. 12. Data collection process

Table 1. Sample distribution in the dataset

Activity	Training set	Test set
Left blink (L)	200	50
Right blink (R)	200	50
Double blink (B)	200	50
Neutral (N)	200	50
Total	800	200

2.2.2. Classification model

The training model is designed to classify blink signals acquired from two channels, each with a length of 640 samples. The objective is to identify four different input signal states: L, R, B, and N. The data are normalized, enhanced through feature processing, and fed into a hybrid CBA-FusionNet model that integrates CNN, BiLSTM, and an Attention mechanism to maximize classification performance.

The model follows a dual-input architecture. One branch processes the raw signals through Conv1D layers to extract temporal features, followed by a BiLSTM layer and a custom Attention mechanism to capture bidirectional dependencies and emphasize the most informative signal segments. The other branch processes high-level statistical features extracted from both channels, using a Dense layer for feature learning and dimensionality reduction. The outputs of the two branches are then concatenated and fed into a final Dense layer with a softmax activation function to produce four-class classification results.

This architecture combines 1D-CNN, BiLSTM, and an Attention mechanism to automatically extract features from blink signals (Fig. 13). Three consecutive 1D-CNN blocks with increasing filters (64, 128, 256), along with Batch Normalization, LeakyReLU, MaxPooling1D, and Dropout, are used to capture local temporal features and stabilize training. The extracted features are then processed by a bidirectional BiLSTM (64 hidden units per direction) to learn temporal dependencies, followed by a custom Attention layer that emphasizes important time intervals and generates a final 128-dimensional feature vector for the first branch.

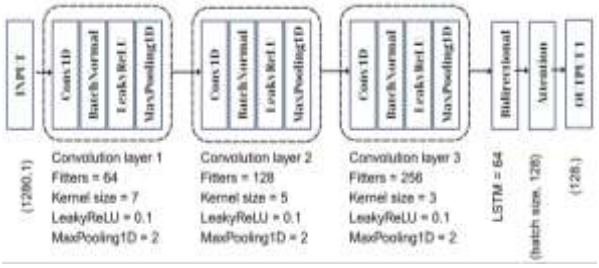


Fig. 13. First-branch network model for raw signal processing

In the second branch (Fig. 14), a Dense layer combined with Dropout is used to learn from manually extracted statistical features of the blink signals. The input is a (batch_size, 49) feature vector containing metrics such as mean, standard deviation, energy, FFT, ZCR, and inter-channel correlation. This input is passed through a 64-unit Dense layer with ReLU activation to model nonlinear relationships, followed by a Dropout layer (rate is 0.3) to reduce overfitting. The branch outputs a feature vector of size (batch_size, 64).

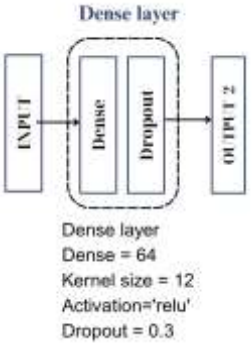


Fig. 14. Second-branch network model for feature processing

The outputs of the two branches are concatenated into a (batch_size, 192) vector, then passed through a 64-unit Dense layer with ReLU, followed by Dropout (0.3) to reduce overfitting (Fig. 15). A final Dense layer with 4 neurons and softmax activation produces a (batch_size, 4) output representing the probabilities of the four classes: L, R, B, and N.

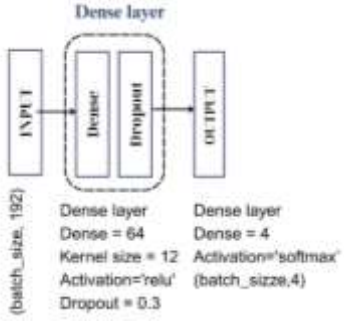


Fig. 15. Combined dual-branch network model

The model also applies EarlyStopping to prevent overfitting by halting training when performance no longer improves, and L2 regularization in Conv1D and Dense layers to control weight values, smooth the model, and enhance generalization.

3. Result and Discussion

3.1. Hardware Implementation Results

The EEG acquisition and processing circuit has a size of 4cm × 4 cm, as shown in Fig. 16. Specifically, the first circuit includes three electrodes: a signal acquisition electrode, a reference electrode, and a DRL electrode. The second circuit uses only two electrodes: one signal acquisition electrode and one reference electrode, while the DRL electrode is shared by both circuits according to the previously presented design.

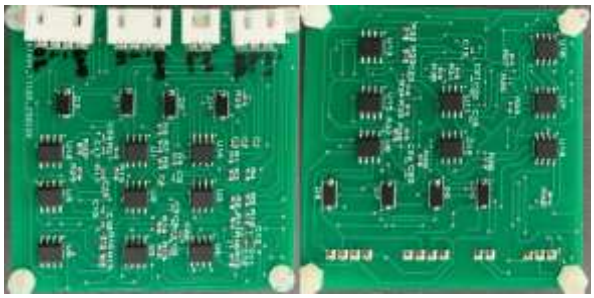


Fig. 16. Front and back of circuit

As shown in Fig. 17, to acquire left-eye blink signals, the first circuit uses three electrodes: Fp1 (IN1) placed above the left eyebrow, A1 (IN2) placed on the left ear, and a shared DRL electrode attached to either leg. Similarly, for right-eye signal acquisition, the second circuit uses Fp2 (IN1) above the right eyebrow and A2 (IN2) on the right ear, with the same DRL electrode shared and attached to either leg.

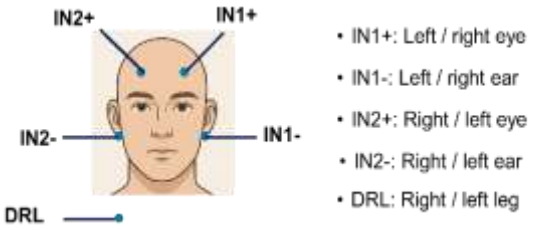


Fig. 17. Electrodes placement diagram



Fig. 18. Side views of the device enclosure



Fig. 19. Illustration of the device placement on the arm and the electrode-integrated headband

The assembled acquisition device includes a voltage divider circuit, battery, and Arduino integrated into a 3D-printed enclosure, as shown in Fig. 18. Fig. 19 illustrates the placement of the EEG acquisition device on the user's arm. The device is secured using two adjustable elastic straps, ensuring stability during data collection while maintaining user comfort and preventing unwanted movement. Fig. 18 also shows the headband with integrated electrodes. Gold-plated Emotiv EPOC+ electrodes are used to ensure good contact and high signal quality. The elastic headband is designed to fit various head sizes while firmly securing the electrodes during operation.

3.2. Electroencephalogram Signal Acquisition and Processing Results

Blink signals typically have larger amplitudes than other EEG signals due to the strong electrical potentials generated by eye muscle activity. They often appear as sharp peaks or spike-like waveforms. The following figure shows the raw, unprocessed signal, including noise components and original characteristics, as acquired and visualized in MATLAB.

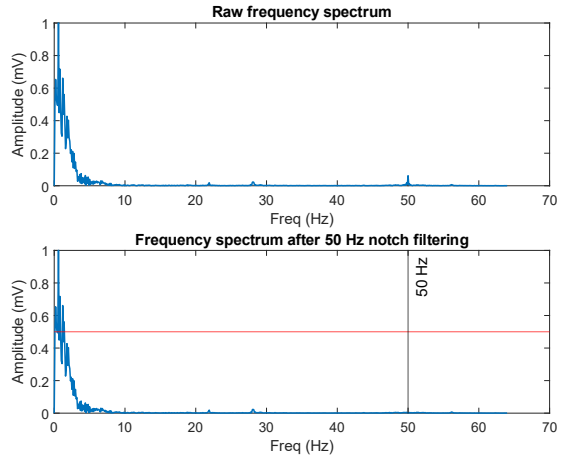


Fig. 20. Frequency spectrum of the signal before and after 50 Hz filtering

Fig. 20 shows the EEG frequency spectrum before and after applying a 50 Hz Notch filter. In the original spectrum (top), most signal energy is concentrated below 10 Hz, corresponding to important physiological bands such as Delta, Theta, and Alpha. However, a clear interference peak appears around 50 Hz due to power-line noise.

After applying the 50 Hz Notch filter (bottom), this interference component is effectively removed, as indicated by the disappearance of the 50 Hz peak. The low-frequency EEG components remain largely preserved, demonstrating that the filter suppresses noise without distorting the main signal. Removing the 50 Hz interference improves the accuracy of EEG processing tasks such as blink detection and brain state classification.

Fig. 21 shows the 10-second blink signal recorded without using the DRL electrode. The signal contains significant background noise, with dense small oscillations across the waveform. Blink events are hardly distinguishable, and noise amplitudes exceed 400 mV, indicating strong power-line and external interference. Without the DRL electrode, the system's ability to suppress common-mode noise is greatly reduced. Since DRL stabilizes the reference voltage and minimizes environmental interference, its absence significantly degrades signal quality, making subsequent processing and classification more difficult.

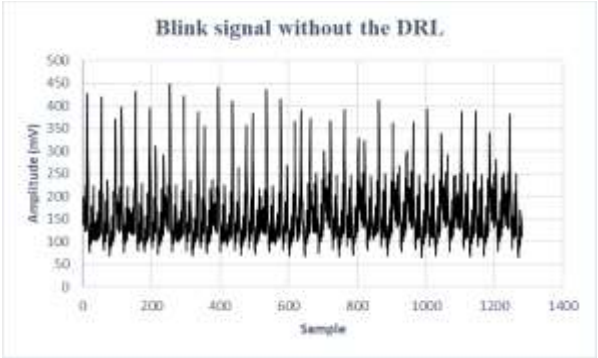


Fig. 21. Blink signal without the DRL

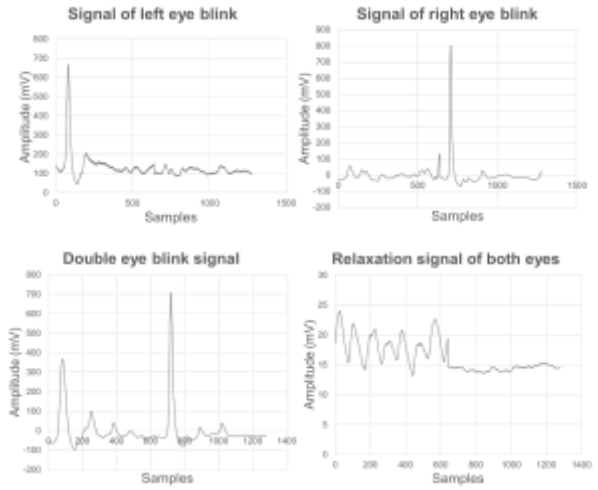


Fig. 22. Acquired signals of left blink, right blink, both-eye blink, and no-blink states

Fig. 22 shows that the EEG signal becomes significantly clearer when the DRL electrode is used compared to when it is not. The blink signal amplitude remains distinct, while background noise is substantially reduced, making it easier to differentiate between the actual signal and noise. This highlights the important role of the DRL electrode in suppressing common-mode noise, particularly 50 Hz power-line interference and unwanted physiological noise.

3.3. Comparison with Other Electroencephalogram Devices

The objective is to evaluate the signal quality of the proposed Eye-Blink EEG (EB-EEG) system by comparing it with signals acquired from the Emotiv EPOC+, thereby assessing its accuracy and practical suitability. For comparison, both signals are processed using a 4th-order Butterworth low-pass filter (cutoff at 4 Hz) to remove high-frequency noise, then normalized (mean removal) and amplitude-scaled for visual consistency. Time-lag alignment is applied to synchronize peak positions, and Signal-to-Noise Ratio (SNR) is calculated to quantify noise levels.

As shown in Fig. 23, the EB-EEG (blue) and Emotiv EPOC+ (red) signals exhibit strong synchronization at the blink peak. Although their amplitudes differ significantly (approximately 440 µV for Emotiv and approximately 440 mV for EB-EEG) due to different gain configurations, the post-peak waveform shapes are highly similar, indicating accurate physiological signal acquisition by the proposed system. Background oscillations remain low in both cases, demonstrating effective noise suppression. Overall, the EB-EEG system reliably detects left blink events with clear signal characteristics and minimal interference.

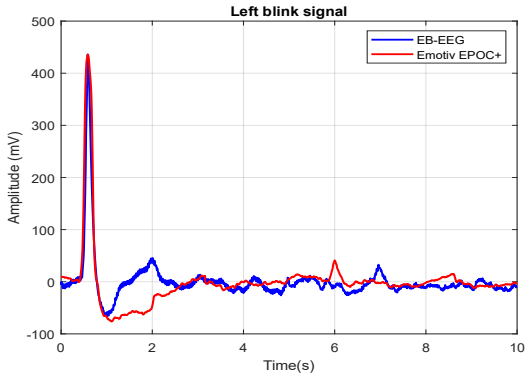


Fig. 23. Left blink signal of the EB-EEG compared with the left blink signal of the Emotiv EPOC+

As shown in Fig. 24, the blink peak (~380 µV) is accurately detected and well aligned in time between the two systems. However, the Emotiv EPOC+ signal exhibits more low-frequency background oscillations, particularly in the 0–5 s and 6–9 s intervals. In contrast, the EB-EEG signal shows lower baseline amplitude and fewer fluctuations, indicating stronger noise suppression, though potentially at the cost of attenuating low-amplitude background brain waves.

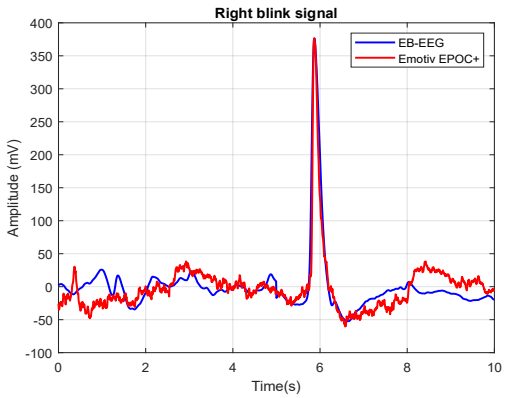


Fig. 24. Right blink signal of the EB-EEG compared with the left blink signal of the Emotiv EPOC+

Table 2 presents the quantitative SNR comparison between the EB-EEG device and Emotiv EPOC+. The average SNR of EB-EEG is slightly higher than that of Emotiv EPOC+ (+0.06 dB) [28], indicating good noise filtering capability. However, some samples show large variations across measurements, reflecting the influence of electrode placement or external noise.

Table 2. Quantitative Evaluation Statistics between the EB-EEG Device and Emotiv EPOC+

Metric	EB - EEG	Emotiv EPOC+
Average SNR	9.59 dB	9.53 dB
Highest SNR	10.33 dB	10.46 dB
Lowest SNR	8.95 dB	7.96 dB

Fig. 25 illustrates the SNR values across samples, where the horizontal axis represents the sample index and the vertical axis shows the SNR. The results indicate that both devices achieve SNR values in the range of 9–10.5 dB. However, EB-EEG demonstrates greater stability with smaller fluctuations across samples, whereas Emotiv EPOC+ exhibits larger variations, with some samples dropping to nearly 8 dB.

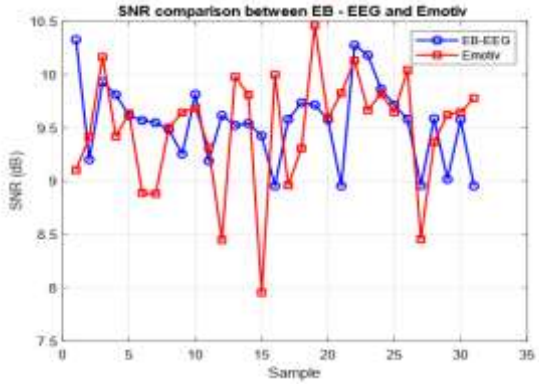
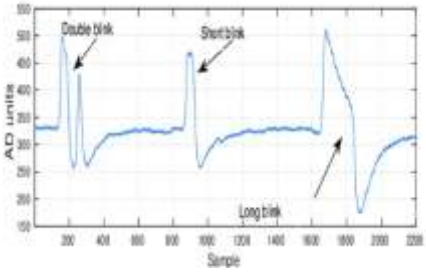
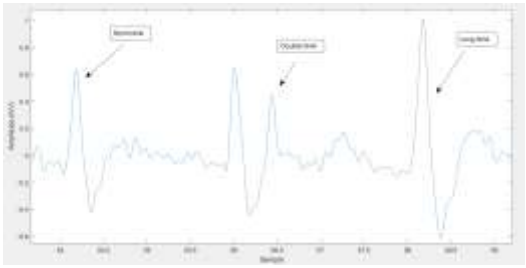


Fig. 25. SNR Comparison between EB-EEG and Emotiv EPOC+

EB-EEG demonstrates relatively good EEG acquisition performance, with a high and stable average SNR. However, its sensitivity in detecting all blink events is lower compared to Emotiv EPOC+. Therefore, EB-EEG is more suitable for applications requiring clear and strong signal detection (such as device control via intentional blinks), whereas Emotiv EPOC+ is better suited for tasks demanding higher sensitivity, such as mental state analysis or emotion recognition.

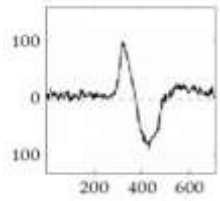


(a)

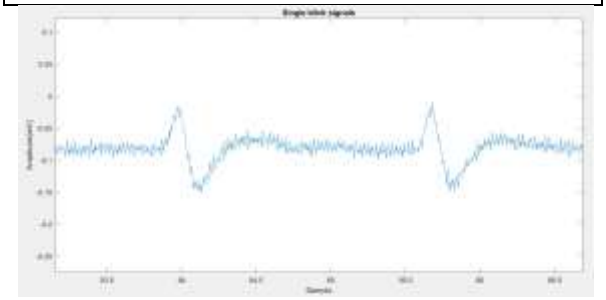


(b)

Fig. 26. Comparison of blink signals: (a) EEG signal acquired using the Neurosky Mindwave device, sampling rate 512 Hz, bandpass filtered from 0.5–100 Hz; (b) EEG signal acquired from the EB-EEG device, sampling rate 128 Hz, digitally bandpass filtered from 0.4–106 Hz



(a)



(b)

Fig. 27. Comparison of single-blink signals: (a) A single-blink signal used for machine learning training in the HMI system, acquired by the Neurosky Mindwave device; (b) A single-blink signal acquired from the EB-EEG device

From Fig. 26, both the Neurosky Mindwave [29, 30] and the EB-EEG devices capture characteristic blink patterns such as short, long, and double blinks. However, although the EB-EEG signal shows relatively clear amplitudes, it contains more background noise compared to the Neurosky device, likely due to the more optimized filtering and noise-reduction system of the commercial device.

Fig. 27 shows that the single-blink waveform of the EB-EEG is relatively similar to the reference signal from the Neurosky Mindwave [31]. The peak and the return to baseline are clearly observed, demonstrating that the EB-EEG can reliably capture blink characteristics, although the signal appears slightly rougher.

3.4. Results of Electroencephalogram Signal Classification for Blink Activities

After developing and training the deep learning model for blink signal classification, the system achieved promising results on the test dataset. The CBA-FusionNet model combines 1D-CNN for feature extraction, BiLSTM for capturing temporal dependencies, and an Attention mechanism to emphasize important signal segments. Additionally, two auxiliary branches process statistical and inter-channel features to enhance generalization capability. The model was trained using the configuration parameters shown in Table 3.

Table 3. Model training parameters

Parameters	**Value**
Total epochs	100
Batch size	32
Optimizer	Adam
Loss function	Local Loss
Callback	EarlyStopping (patience=10), ReduceLROnPlateau

The results indicate that the model performs very well in recognizing blink gestures from EEG signals, achieving an accuracy of 0.96, with Precision, Recall, and F1-score all ranging from 0.95 to 0.97 across the four classes, as detailed in Table 4. This suggests that the model not only classifies most samples correctly but also maintains a strong balance between correct detection and class discrimination. In particular, class R achieves the highest recall, showing that the model identifies this signal especially well, while class N has slightly lower precision, indicating that some samples are still being misclassified into this class. Overall, the results are highly promising and demonstrate stable gesture recognition with strong potential for EEG-based control applications.

Table 4. Training results

Class	Precision	Recall	F1-score
L	0.98	0.94	0.96
R	0.96	0.98	0.97
B	0.96	0.96	0.96
N	0.94	0.96	0.95

In Fig. 28, both training and validation accuracy increase rapidly during the first 15 epochs and stabilize around 96–98%, indicating effective learning without overfitting. Meanwhile, the training and validation loss decrease sharply within the first 10 epochs and gradually converge to a low value (approximately 0.05), demonstrating efficient optimization and good generalization performance.

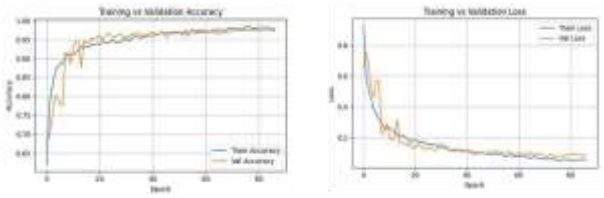


Fig. 28. Accuracy and loss curves of the training and validation sets

Fig. 29 presents the confusion matrix of the model evaluated on the test set with four classes: L, R, B, and N, illustrating correct and misclassified samples across classes. Specifically, class L achieved 47/50 correct predictions (94%), class R 49/50 (98%), class B 48/50 (96%), and class N 48/50 (96%).

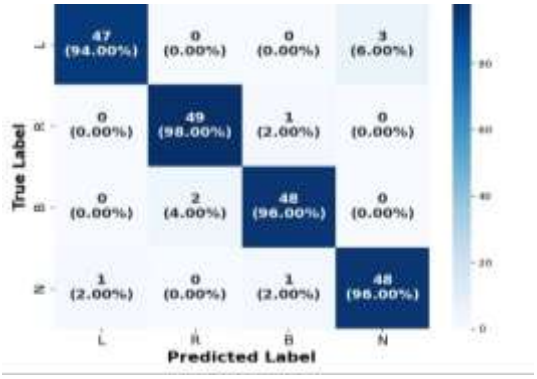


Fig. 29. Confusion matrix

Table 5. Experimental Results

Class	Number of correct predictions	Number of incorrect predictions	Accuracy
L	27	3	0.9
R	25	5	0.83
B	28	2	0.93
N	29	1	0.96

In addition, the model was deployed in an experimental setup to evaluate its real-world performance. Specifically, data were collected and predictions were generated every 5 seconds. The participant sat steadily on a chair; the first 5 seconds were used for relaxation to record baseline signals, followed by performing each type of blink movement, with 30 repetitions per type to collect data for further analysis and prediction. The results are presented in Table 5. From Table 5, the model demonstrates good experimental performance across four classes (30 samples per class). Class N achieved the highest accuracy (96%), followed by B (93%) and L (90%), while R obtained the lowest accuracy (83%). The overall average accuracy of the model reached 90.5%, indicating that the system operates stably and effectively under real-world conditions, although class R still exhibits a relatively higher misclassification rate compared to the other classes.

4. Conclusion and Future Work

This study successfully designed and developed a low-cost two-channel EEG acquisition device for detecting blink activities, which can be comfortably worn and operates stably under real-world conditions. The recorded blink signals clearly exhibited characteristic sharp peaks and could be stored for further processing and analysis. The collected dataset was used to train a CNN-based classification model for recognizing four eye-movement labels (L, R, B, and N), achieving high classification accuracy. Experimental results showed that the proposed system achieved an average accuracy of 96% during training and 90.5% in real-world testing, confirming the feasibility of the system for non-contact control applications as well as serving as an initial step toward Brain–Computer Interface (BCI) development.

Although promising results were achieved, the proposed system still presents several limitations in both hardware design and signal acquisition protocol. The collected dataset and the number of participants were relatively limited, which may not fully represent the diversity of EEG signals in real-world scenarios. In addition, the current study only evaluated a CBA-FusionNet architecture without comparison to other CNN or deep learning models. Future work will focus on miniaturizing the device, selecting components that support multi-channel expansion, and designing a dedicated headband to provide more stable electrode placement. Furthermore, digital filtering techniques need to be improved to better distinguish intentional and involuntary blink activities, enhance recognition accuracy, and optimize the signal acquisition protocol. Expanding the dataset, increasing the number of participants, and investigating more advanced deep learning architectures will also be considered to improve the robustness and generalization capability of the proposed EEG classification system.

Acknowledgments

This work is supported by Ho Chi Minh City University of Technology and Engineering (HCM-UTE) under Grant No. T2025-190.

References

[1] A. Chaddad, Y. Wu, R. Kateb, and A. Bouridane, Electroencephalography Signal Processing: A Comprehensive Review and Analysis of Methods and Techniques, Sensors, vol. 23, no. 14, pp. 1–27, 2023, Art. no. 6434. https://doi.org/10.3390/s23146434

[2] M. K. Islam and A. Rastegarnia, Editorial: Recent advances in EEG (non-invasive) based BCI applications, Frontiers in Computational Neuroscience, vol. 17, 2023, Art. no. 1151852. https://doi.org/10.3389/fncom.2023.1151852

[3] M. Soufineyestani, D. Dowling, and A. Khan, Electroencephalography (EEG) Technology Applications and Available Devices, Applied Sciences, vol. 10, no. 21, pp. 1–23, 2020, Art. no. 7453. https://doi.org/10.3390/app10217453

[4] E. Bullmore and O. Sporns, Complex brain networks: Graph theoretical analysis of structural and functional systems, Nature Reviews Neuroscience, vol. 10, no. 3, pp. 186–198, Mar. 2009. https://doi.org/10.1038/nrn2575

[5] R. Salinas, E. Schachter, and M. Miranda, Recognition and real-Time detection of blinking eyes on electroencephalographic signals using wavelet transform, in Proceedings of Progress in Pattern Recognition, Image Analysis, Computer Vision, and Applications, Berlin, Heidelberg, pp. 682–690, 2012. https://doi.org/10.1007/978-3-642-33275-3_84

[6] N. Sciaraffa, G. Borghini, G. D. Flumeri, F. Cincotti, F. Babiloni, and P. Aricò, Joint Analysis of Eye Blinks and Brain Activity to Investigate Attentional Demand during a Visual Search Task, Brain Sciences, vol. 11, no. 5, pp. 1–20, 2021, Art. no. 562. https://doi.org/10.3390/brainsci11050562

[7] S. Sattari, R. Kenny, C. C. Liu, S. G. Hajra, G. A. Dumont, and N. Virji-Babul, Blink-related EEG oscillations are neurophysiological indicators of subconcussive head impacts in female soccer players: A preliminary study, Frontiers in Human Neuroscience, vol. 17, pp. 1–10, 2023, Art. no. 1208498. https://doi.org/10.3389/fnhum.2023.1208498

[8] M. Orban, M. Elsamanty, K. Guo, S. Zhang, and H. Yang, A Review of Brain Activity and EEG-Based Brain–Computer Interfaces for Rehabilitation Application, Bioengineering, vol. 9, no. 12, pp. 1–22, 2022. https://doi.org/10.3390/bioengineering9120768

[9] M. A. Lebedev and M. A. L. Nicolelis, Brain-Machine Interfaces: From Basic Science to Neuroprostheses and Neurorehabilitation, Physiological Reviews, vol. 97, no. 2, pp. 767–837, Apr. 2017. https://doi.org/10.1152/physrev.00027.2016

[10] X. Mao, M. Li, W. Li, L. Niu, B. Xian, M. Zeng, and G. Chen, Progress in EEG-Based Brain Robot Interaction Systems, Computational Intelligence and Neuroscience, vol. 2017, pp. 1–25, 2017, Art. no. 1742862. https://doi.org/10.1155/2017/1742862

[11] V. Peterson, C. Galván, H. Hernández, and R. Spies, A feasibility study of a complete low-cost consumer-grade brain-computer interface system, Heliyon, vol. 6, no. 3, pp. 1–12, 2020, Art. no. e03425. https://doi.org/10.1016/j.heliyon.2020.e03425

[12] N. Tibrewal, N. Leeuwis, and M. Alimardani, Classification of motor imagery EEG using deep learning increases performance in inefficient BCI users, PLOS ONE, vol. 17, no. 7, pp. 1–18, 2022, Art. no. e0268880. https://doi.org/10.1371/journal.pone.0268880

[13] A. Craik, Y. He, and J. L. Contreras-Vidal, Deep learning for electroencephalogram (EEG) classification tasks: A review, Journal of Neural Engineering, vol. 16, no. 3, pp. 1–28, 2019m, Art. no. 031001. https://doi.org/10.1088/1741-2552/ab0ab5

[14] V. J. Lawhern, A. J. Solon, N. R. Waytowich, S. M. Gordon, C. P. Hung, and B. J. Lance, EEGNet: A compact convolutional neural network for EEG-based brain–computer interfaces, Journal of Neural Engineering, vol. 15, no. 5, pp. 1–30, 2018, Art. no. 056013. https://doi.org/10.1088/1741-2552/aace8c

[15] A. Das, S. Singh, J. Kim, T. A. Ahanger, and A. A. Pise, Enhanced EEG signal classification in brain computer interfaces using hybrid deep learning models, Scientific Reports, vol. 15, no. 1, pp. 1–20, 2025, Art. no. 27161. https://doi.org/10.1038/s41598-025-07427-2

[16] J. I. Padilla-Buritica, J. V. Hurtado, and G. Castellanos-Dominguez, Supervised piecewise network connectivity analysis for enhanced confidence of auditory oddball tasks, Biomedical Signal Processing and Control, vol. 52, pp. 341–346, 2019. https://doi.org/10.1016/j.bspc.2019.04.020

[17] T. Bayan, D. Das, and N. Deb, Deep Hybrid CNN-BiLSTM-Attention Model for EEG Classification Using Wavelet Features, Annals of Neurosciences, pp. 1–10, Jan. 2026. https://doi.org/10.1177/09727531251396337

[18] J. Zhang, J. Li, Z. Huang, D. Huang, H. Yu, and Z. Li, Recent progress in wearable brain–computer interface (BCI) devices based on electroencephalogram (EEG) for medical applications: A review, Health Data Science, vol. 3, pp. 1–15, 2023, Art. no. 0096. https://doi.org/10.34133/hds.0096

[19] M. Rashid, N. Sulaiman, A. P. P. Abdul Majeed, R. M. Musa, A. F. Ab. Nasir, B. S. Bari, and S. Khatun, Current status, challenges, and possible solutions of EEG-based brain-computer interface: A comprehensive review, Frontiers in Neurorobotics, vol. 14, pp. 1–35, 2020, Art. no. 25. https://doi.org/10.3389/fnbot.2020.00025

[20] S. N. Abdulkader, A. Atia, and M.-S. M. Mostafa, Brain computer interfacing: Applications and challenges,

Egyptian Informatics Journal, vol. 16, no. 2, pp. 213–230, 2015. https://doi.org/10.1016/j.eij.2015.06.002

[21] J. L. M. Kumar, M. Rashid, R. M. Musa, M. A. M. Razman, N. Sulaiman, R. Jailani, and A. P. P. Abdul Majeed, The classification of EEG-based winking signals: A transfer learning and random forest pipeline, PeerJ, vol. 9, pp. 1–16, 2021, Art. no. e11182. https://doi.org/10.7717/peerj.11182

[22] M. Rashida and M. A. Habib, Quantitative EEG features and machine learning classifiers for eye-blink artifact detection: A comparative study, Neuroscience Informatics, vol. 3, no. 1, pp. 1–8, 2023, Art. no. 100115. https://doi.org/10.1016/j.neuri.2022.100115

[23] M. Rabbani, N. U. S. Sabith, A. Parida, I. Iqbal, S. M. Mamun, R. A. Khan, F. Ahmed, and S. I. Ahamed, EEG based real time classification of consecutive two eye blinks for brain computer interface applications, Scientific Reports, vol. 15, no. 1, pp. 1–21, 2025, Art. no. 21007. https://doi.org/10.1038/s41598-025-07205-0

[24] D. Das, M. H. Chowdhury, A. Chowdhury, K. Hasan, Q. D. Hossain, and R. C. C. Cheung, Application Specific Reconfigurable Processor for Eyeblink Detection from Dual-Channel EOG Signal, Journal of Low Power Electronics and Applications, vol. 13, no. 4, pp. 1–16, 2023, Art. no. 61. https://doi.org/10.3390/jlpea13040061

[25] R. Mahajan and B. I. Morshed, Unsupervised Eye Blink Artifact Denoising of EEG Data with Modified Multiscale Sample Entropy, Kurtosis, and Wavelet-ICA, IEEE Journal of Biomedical and Health Informatics, vol. 19, no. 1, pp. 158–165, 2015. https://doi.org/10.1109/JBHI.2014.2333010

[26] G. D. Gargiulo, P. Bifulco, M. Cesarelli, A. McEwan, A. Nikpour, C. Jin, U. Gunawardana, N. Sreenivasan, A. Wabnitz, and T. J. Hamilton, Fully Open-Access Passive Dry Electrodes BIOADC: Open-Electroencephalography (EEG) Re-Invented, Sensors, vol. 19, no. 4, pp. 1–16, 2019, Art. no. 772. https://doi.org/10.3390/s19040772

[27] R. Mahajan and B. I. Morshed, Performance analysis of a DRL-less AFE for battery-powered wearable EEG, Measurement, vol. 90, no. 2016, pp. 583–591, Aug. 2016. https://doi.org/10.1016/j.measurement.2016.04.040

[28] A. J. Molina-Cantero, C. Lebrato-Vázquez, M. Merino-Monge, R. Quesada-Tabares, J. A. Castro-García, and I. M. Gómez-González, Communication Technologies Based on Voluntary Blinks: Assessment and Design, IEEE Access, vol. 7, pp. 70770–70798, 2019. https://doi.org/10.1109/ACCESS.2019.2919324

[29] S. Morshad, M. R. Mazumder, and F. Ahmed, Analysis of Brain Wave Data Using Neurosky Mindwave Mobile II, presented at the Proceedings of the International Conference on Computing Advancements, Dhaka, Bangladesh, 2020. https://doi.org/10.1145/3377049.3377053

[30] H. Al-Kaf, A. Khandoker, K. Khalaf, and H. F. Jelinek, NeuroSky Mindwave Mobile Headset 2 as an Intervention for Reduction of Stress and Anxiety Measured with Pulse Rate Variability, in Proceedings of 2020 Computing in Cardiology, pp. 1–4, 2020. https://doi.org/10.22489/CinC.2020.350

[31] J. F. Wu, A. M. S. Ang, K. M. Tsui, H. C. Wu, Y. S. Hung, Y. Hu, J. N. F. Mak, S. C. Chan, and Z. G. Zhang, Efficient Implementation and Design of a New Single-Channel Electrooculography-Based Human–Machine Interface System, IEEE Transactions on Circuits and Systems II: Express Briefs, vol. 62, no. 2, pp. 179–183, 2015. https://doi.org/10.1109/TCSII.2014.2368617